remote sensing

MDPI

Technical Note

Landscape-Scale Crop Lodging Assessment across Iowa and Illinois Using Synthetic Aperture Radar (SAR) Images

Olaniyi A. Ajadi [1,*], Heming Liao [1], Jason Jaacks [1], Alfredo Delos Santos [1], Siva P. Kumpatla [1], Rinkal Patel [2] and Anu Swatantran [1]

[1] Research & Development Corteva Agriscience™, 7000 NW 62nd Avenue, Johnston, IA 50131, USA; heming.liao@corteva.com (H.L.); jason.jaacks@corteva.com (J.J.); alfredo.delossantos@corteva.com (A.D.S.); siva.kumpatla@corteva.com (S.P.K.); anuradha.swatantran@corteva.com (A.S.)

[2] Granular 8700 Crescent Chase, Johnston, IA 50131, USA; rinkalpatel@granular.ag

* Correspondence: olaniyi.ajadi@corteva.com; Tel.: +1-(515)-535-2983

Received: 30 October 2020; Accepted: 25 November 2020; Published: 27 November 2020

Abstract: Crop lodging, the tilting of stems from their natural upright position, usually occurs after a heavy storm event. Since lodging of a crop seriously affects its yield, rapid assessment of crop lodging is valuable for farmers, policymakers, agronomists, insurance companies, and relief workers. Synthetic Aperture Radar (SAR) sensors have been recognized as valuable data sources for mapping lodging extent because of their good penetrating power and high-resolution remote sensing ability. Compared to other sources, SAR's weather and illumination independence and large area coverage at fine spatial resolution (3 m to 20 m) support frequent and detailed observations. Because of these advantages, SAR has the potential in supporting near real-time monitoring of lodging in fields when combined with automated image processing. In this study, a method based on change detection using modified Hidden Markov Random Field (HMRF) and Sentinel-1A data were utilized to identify lodging and map its extent. Results obtained have shown that when lodging occurs, the VH polarization's backscatter (σVH) increases between the pre-lodging event image and the post-lodging event image. The increase in σVH is due to the increase in volume scattering and vegetation-soil double bounce scattering resulting from the structural changes in the crop canopy. Using Sentinel-1A images and applying our proposed approach across several fields in Iowa and Illinois, we mapped the extent of the 2020 Derecho (wind storm) lodging disaster. In addition, we separated lodged regions into severely and moderately lodged areas. We estimated that approximately 2.56 million acres of corn and 1.27 million acres of soybean were lodged. Further analysis also showed the separation between un-lodged (healthy) fields and lodged fields. The observations in this study can guide future use of SAR-based information for operational crop lodging assessment.

Keywords: Synthetic Aperture Radar; SAR; lodging; Hidden Markov Random Field; HMRF; CDL; corn; soybean; crop Monitoring; crop management

1. Introduction

With the increase in global population and the increase in food demand, the monitoring of agricultural activities has been of utmost importance. The increasing frequency and intensity of extreme weather events have also made monitoring of agricultural fields very critical. Lodging, the tilting of plant stems from their natural upright position, is a major yield limiting factor to crops such as corn, wheat, and barley [1–3]. Corn is vulnerable to lodging during its growing stages, particularly between early to late vegetative period [4]. Lodging in corn could be as a result

of insufficient root growth due to soil compaction, or due to increased occurrence of heavy rain and derechos (wind storms). According to the National Oceanic and Atmospheric Administration (NOAA), derechos are straight-line windstorms that are associated with a fast-moving group of severe thunderstorms. The winds are destructive and can be as strong as those found in tornadoes and hurricanes. Derecho lodging results in serious damage to crop growth and development as it impedes the circulation of water and nutrients in the plant which in turn suppresses photosynthesis, leading to deterioration of grain quality and total yield loss [5]. For a more comprehensive overview on the mechanics of lodging, factors affecting lodging, and crop yield response to lodging, the reader is referred to Chauhan, et al. [6]. Lodging also reduces grower's profitability and, for this reason, it is important to detect lodging quickly, map its extent, and quantitatively measure its severity. Accurate and timely mapping of lodged fields can help guide farmers during harvest operations, help crop insurance companies during crop loss assessment, and can improve crop yield forecasts [7].

Mapping of lodged fields is typically based on visual inspection (field-based approach). However, this approach is extremely laborious, time consuming, and is infeasible for large areas. In recent years, remote sensing has been used for mapping lodging since it offers a more scalable approach and is also cost effective. Multi-temporal images acquired by optical [8,9] and radar [10,11] sensors have routinely been applied for lodging identification. Since these two sensor types have their unique sensitivity and imaging characteristics, their performance in the mapping of lodging varies.

Recently, synthetic aperture radar (SAR) data have gained considerable interest in lodging applications because SAR is an active sensor, operating without regard to weather, smoke, cloud cover, or daylight [12]. SAR sensors offer a clear advantage because of their unique scattering sensitivity to crop structure and large area coverage.

In Chauhan, et al. [8], the authors used time series of SAR backscatter, SAR coherence, and spectral reflectance derived from Sentinel-1 and Sentinel-2 data to detect lodging incidence and understand the effect of lodging in wheat. The most reliable discriminators for differentiating lodged wheat from healthy wheat were Sentinel-2 red edge band (740 nm), Sentinel-2 near infrared band (865 nm), and Sentinel-1 VH backscatter. Shu, et al. [13] have used the dual-polarization of Sentinel-1A data to develop a change detection method using plant height before and after lodging in maize to calculate the lodging angle and monitor the lodging degree. The results showed that VV backscatter was sensitive to lodged maize while the ratio of VH to VV backscatter was sensitive to non-lodged maize. In a similar study, Chauhan, et al. [14], explored the advantage of multi-sensor SAR data (Sentinel-1 and RADARSAT-2) to develop a quantitative approach to detect crop lodging stages (moderate, severe, and very severe) based on the crop angle of inclination. Quantitative relationships using support vector regression (SVR) models were established between remote sensing derived metrics from Sentinel-1 and RADARSAT-2 timeseries and field measured crop angle of inclination values [14].

While several researchers have predominantly used the single and dual-polarization of Sentinel-1 to address crop lodging, others have focused on using the multi-configuration (multi-polarization and multi-incidence angle) data from RADARSAT-2. For example, Yang, et al. [15] used a time series of Radarsat-2 images and target decomposition techniques to derive a set of polarimetric features and backscattering intensity features to compare typical lodged fields and normal fields. In their study, they found that polarimetric ratios (especially those based on odd/double scattering) were sensitive in distinguishing lodged and normal fields. In a different study, Chen, et al. [16] used polarimetric features from Polarimetric SAR (PolSAR) to identify sugarcane lodging. The authors found that several polarimetric features, such as horizontal transmit and vertical receive (HV) intensity, double-bounce scattering, and volume scattering derived from RADARSAT-2 data were helpful in sugarcane lodging identification.

Despite these and other studies carried out throughout the last decade, the integration of SAR remote sensing into routine mapping of lodging and severity assessment remains difficult for the following reasons: (a) The acquisition of SAR dataset to coincide with the specific date of lodging is not always feasible; (b) The heterogeneous distribution of lodging makes it difficult to be detected

with SAR and also, in particular, in order to map lodging precisely, the size of the lodged field must be larger than the spatial resolution of the SAR sensor; (c) The mapping of lodging over large spatial extent and determination of lodging rate; (d) The acquisition of ground truth data (known lodged fields) to evaluate lodging severity can itself be an overwhelming task as it is extremely labor intensive and time consuming; (e) The accuracy assessment of the lodging severity also has some shortcomings since there are no standard scales to quantify lodging into categories such as severe, moderate, or mild.

To address and overcome some of these challenges, we used the 2020 Derecho event in Midwest U.S. as a case-study to evaluate SAR for large-scale lodging detection and mapping. The main objectives and novelty of this study are to:

(1) Understand the changes in backscatter over large-scale lodged fields and how to use the backscatter to classify lodging into severe or moderate categories.
(2) Generate large-scale spatial extent maps of lodging using a change detection approach modified from our previous study [17] and determine the lodging rate (lodged crop per unit area) using the USDA's Crop Data Layer (CDL) map.
(3) Qualitatively explore the relationship between high wind speed and lodged fields.
(4) Explore the capability of Sentinel-1A over an optical dataset like the one from Landsat-8.
(5) Explore if lodged and un-lodged (healthy) fields differ between the pre-lodging event image and post-lodging event image.

In this paper, the proposed change detection method for lodging utilizes the concept of ratio image generation. The generation of ratio images suppresses background information while enhancing change information [17]. The generated ratio images were filtered using a non-local means filter [18,19] and classified into different classes using the Hidden Markov Random Field (HMRF). The HMRF considers the contextual information of neighboring pixels (i.e., a neighboring pixel is expected to have similar intensities and similar class labels) during classification. Published methods differ in their approach to extract change detection map. In the work done by Kasetkasem and Varshney [20], the authors used a MRF to model noiseless images for an optimal change image using the maximum a posteriori probability computation and the simulated annealing (SA) algorithm. In Zhao, et al. [21], the authors combined Voronoi Tessellation (VT) and HMRF based Fuzzy C-Means (FCM) algorithm (VTHMRF-FCM) for texture image segmentation. Similarly, in Yang and Yi [22], a novel method based on applying HMRF and generative adversarial network (GAN) on high-resolution SAR images was used for ship detection. To our knowledge and according to Chauhan, et al. [6], the use of satellite-based change detection for crop lodging is sparse. To date, there is no method available for corn and soybean lodging over large spatial areas.

2. Study Area and Data

2.1. Study Area

This study was carried out in Iowa and Illinois, spanning across 52 counties (Figure 1), covering the region affected by the 2020 Derecho lodging disaster which occurred on 10 August 2020. Iowa and Illinois are located in the Western part of the Corn Belt region of the United States and are part of the top agriculture production states. Iowa has a total agricultural land of 30.6 million acres, accounting for 92% of the state's total land area while Illinois has a total agricultural land of 27 million acres, accounting for 75% of the state's total land area. The two-dominant crops in both states are corn and soybean. Other crops like wheat and winter wheat are also planted but they account for a very small portion of all the cropland. In this study, the estimation of lodging rate (lodged crop per unit area) was only focused on corn and soybean. In Iowa and Illinois, the climate is cold and temperate. In Iowa, the wettest month with the most precipitation is June with an average precipitation of 107 mm and an average temperature of 82 °F, while the driest month is January with an average precipitation of 23 mm of rainfall and an average temperature of 31 °F. In Illinois, the wettest month with the most

precipitation is August in the Northern portion of Illinois with an average precipitation of 89 mm and an average temperature of 82 °F, while the driest month is February with an average precipitation of 49 mm of rainfall and an average temperature of 35 °F.

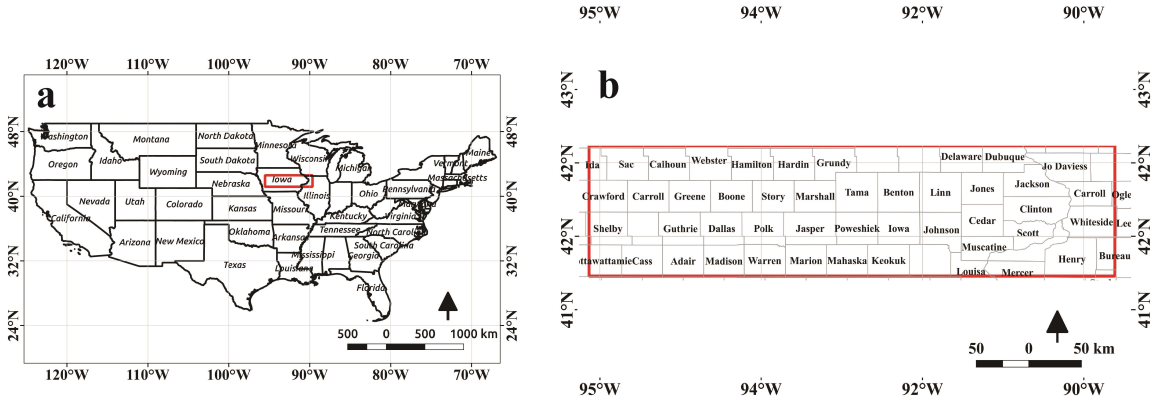

Figure 1. Study area covering (**a**) the region affected by the 2020 Derecho lodging disaster in the states of Iowa and Illinois as shown by the red outline and (**b**) the 52 counties in the affected region.

2.2. Field Data

In order to generate lodged crop per unit area, we used the 2018 CDL map because the 2020 CDL map is not yet available. Another reason for using the 2018 CDL map is that most farmers in Iowa and Illinois perform crop rotation. Fields where farmers consistently performed crop rotations for the last eight years were kept while fields where crop rotations were not consistent for the last eight years were removed. By doing this, we believe that corn and soybeans areas in 2018 should be similar to those of corn and soybean areas in 2020. The CDL data have a spatial resolution of 30 m, includes 132 detailed class labels, and was created from Landsat dataset using a decision tree algorithm trained on field samples [23]. The overall accuracy of the CDL dataset is about 95% for the United States Corn Belt. Apart from the CDL, we collected some ground truth data by field survey. Lodged fields were selected as samples for field observation. Mobile phone GPS was used for positioning the sampling points.

2.3. Remote Sensing Data

During 10 August 2020 and 11 August 2020, a derecho swept through Midwest that caused severe and widespread windstorms with some areas experiencing low-class tornadoes and heavy rain. As part of this, a windstorm was observed in Iowa and Illinois on 10 August 2020. The wind speed in both states ranged between 60 and 100 mph (Figure 2). Wind speed data for this study were acquired from the National Weather Service (NWS). NWS used several sources like Iowa DOT, personal weather station, Automated Surface Observing Systems (ASOS), and Automated Weather Observing Systems (AWOS) to estimate the wind speed data. Since corn and soybean are already in their reproductive stages at the time of the windstorm, high wind speed led to severe lodging.

In order to cover the agricultural areas damaged by the windstorm, we acquired six Sentinel-1A images in Interferometric Wideswath (IW) instrument mode. Our Sentinel-1A images were acquired between 29 July 2020, and 22 August 2020. Each Sentinel-1A image collection had a resolution of 10 m, a dual polarization (VH and VV; V = Vertical, H = Horizontal), and consisted of Level-1 Ground Range Detected (GRD) scenes. As shown in Table 1 and Figure 3, three images were acquired before the lodging event (pre-lodging event) and three images were acquired after the lodging event (post-lodging event).

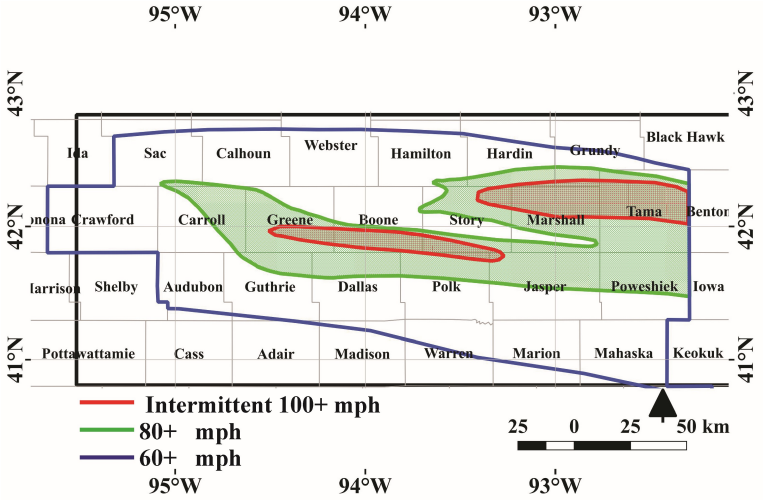

Figure 2. Wind speed data acquired from the National Weather Service (NWS).

Table 1. Details of Sentinel-1A images acquired over Iowa and Illinois.

Date 2015	Flight Direction	Local Standard Time	Incidence Angle	Polarizations	Lodging Event
29 July 2020	ascending	T00:05:15.604Z	30°–46°	VH & VV	Pre-
3 August 2020	ascending	T00:13:42.330Z	30°–46°	VH & VV	Pre-
4 August 2020	ascending	T23:57:18.422Z	30°–46°	VH & VV	Pre-
15 August 2020	ascending	T00:13:42.984Z	30°–46°	VH & VV	Post-
16 August 2020	ascending	T23:57:19.120Z	30°–46°	VH & VV	Post-
22 August 2020	ascending	T00:05:16.823Z	30°–46°	VH & VV	Post-

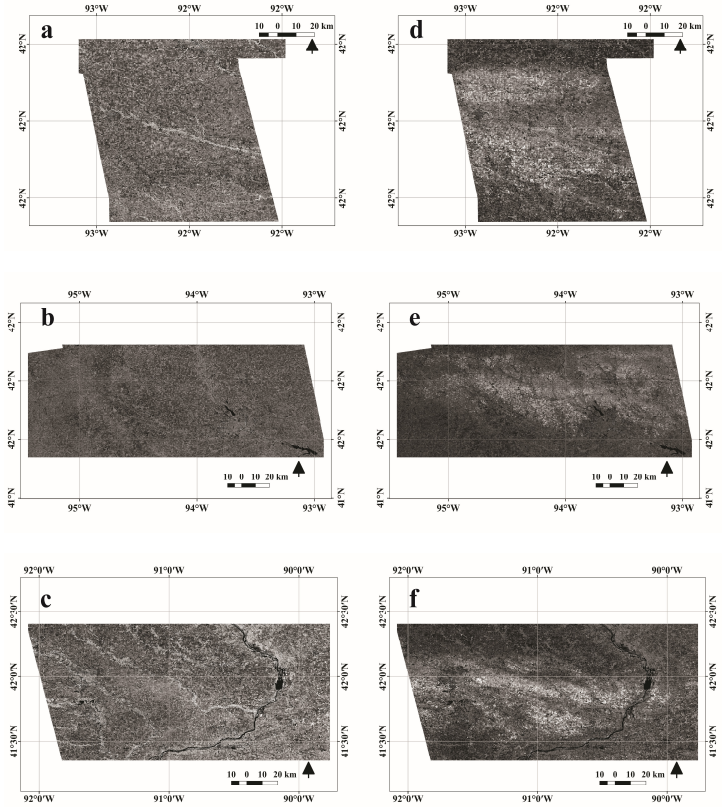

Figure 3. Pre-lodging images acquired on (**a**) 29 July 2020; (**b**) 3 August 2020; and (**c**) 4 August 2020. Post-lodging images acquired on (**d**) 22 August 2020; (**e**) 15 August 2020; and (**f**) 16 August 2020.

3. Methods

A graphical overview of the framework used for this study is illustrated in Figure 4. Major steps of the framework include preprocessing, ratio image formation, and change detection classification approach. All the steps in this paper can be reproduced quickly and all analyses for the study were carried out using python programming language.

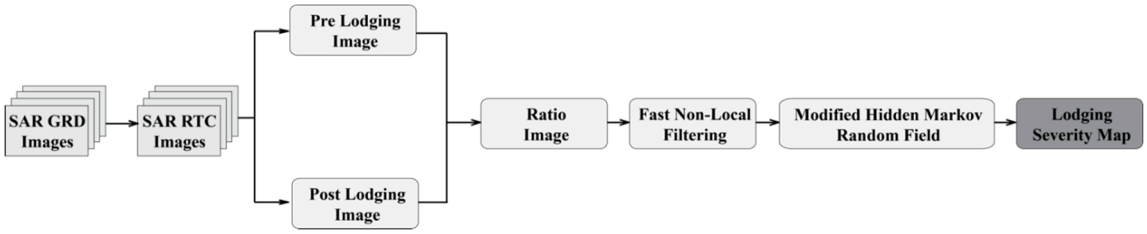

Figure 4. Approach for mapping the 2020 Derecho lodging disaster.

In this paper, our proposed approach requires some parameters to be set beforehand. The parameters that need to be set include (i) the neighborhood size of the non-local means filtering step; (ii) the kernel size of the majority filter; (iii) the structuring element of the morphological filter; and, finally, (iv) the maximum number of allowed change classes. Please note that while we identified optimal settings for these parameters, we found that the performance of our algorithm does not critically depend on the exact choice for these variables. This is true for the following reasons: (i) as non-local means filtering is performed very early in the workflow, the impact of changes in the neighborhood size is mitigated by subsequent processing steps such as the application of mathematical morphology. Hence, we found that varying the neighborhood size from its optimal value changed system performance only slowly; (ii) the increase or decrease in the kernel size of the majority filter slowly decreases our change detection performance, yet this reduction of performance does not become significant unless the kernel size is increased tremendously; (iii) from an analysis of a broad range of data from different change detection projects we found that (1) a 5×5 pixel-sized structuring element of the morphological filter led to the most consistent results; and that (2) change detection performance changed slowly with deviation from the 5×5 pixel setting. Hence, while 5×5 pixel was found to be optimal, the exact choice of the window size is not critical for change detection success; finally, (iv) the maximum number of allowable change classes is a very uncritical variable as it merely sets an upper bound for a subsequent algorithm that automatically determines the number of distinguishable classes in a data set. By presetting this variable to 3 classes we ensure that changes as a result of lodging are captured.

3.1. Image Preprocessing

Sentinel-1A preprocessing was carried out using SeNtinel Application Platform (SNAP) software version 6.0 (https://step.esa.int/main/toolboxes/snap/), an open source common architecture provided by European Space Agency (ESA). The preprocessing step includes orbit file correction, GRD border noise removal, thermal noise removal, calibration, filtering using refined Lee filter, radiometric terrain correction (RTC), and geometric terrain correction (GTC). For more details on the preprocessing step and the importance of RTC, the reader is referred to Ajadi, Meyer and Webley [17].

3.2. Logarithmic Scaling and Ratio Image Formation

While both VH polarization and VV polarization were sensitive to crop lodging assessment, we only used the VH polarization of Sentinel-1A dataset in this study because it depicts crop phenology very well and, moreover, it is very sensitive to crop canopy structure. In order to increase the detectability of lodging and to suppress background information from SAR data, ratio images ($X_{Ris} = [X_{Ri1}, X_{Ri2}, X_{Ri3}]$) were formed (Figures 5 and 6) using the pre-lodging event image and of the

post-lodging event image of similar geometry, respectively (Table 1 and Figure 3). Note that, due to the performed radiometric correction steps, images are not required to come from identical geometries. Also, because the pre-lodging and post-lodging event images are logarithmically scaled, the creation of ratio images is performed as a subtraction operation. Afterwards, a fast-non-local means filtering procedure was applied to all ratio images in order to filter out the speckle noise while preserving the details. The fast-non-local means uses redundant information to reduce noise and restore the original noise-free image by performing a weighted average of pixel values, considering the spatial and intensity similarities between pixels [17].

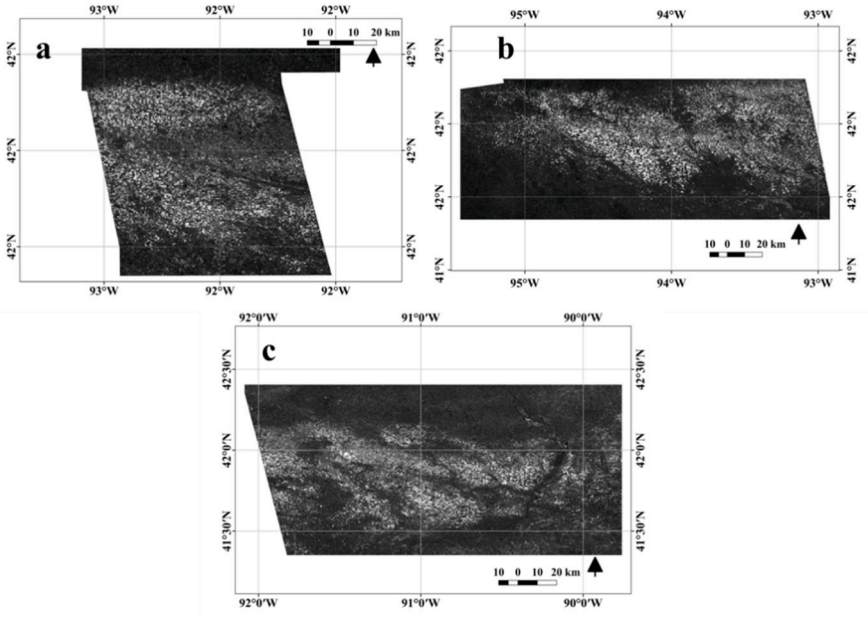

Figure 5. Ratio images generated between (**a**) 29 July 2020 and 22 August 2020; (**b**) 3 August 2020 and 15 August 2020; (**c**) 4 August 2020 and 16 August 2020.

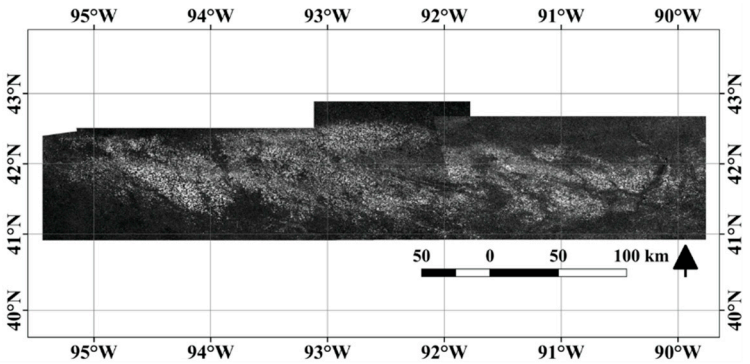

Figure 6. Spatial mosaic of all ratio maps in Figure 5a–c.

3.3. Change Detection Classification Approach

In this study, we employed the Hidden Markov Random Field (HMRF) approach to perform our lodging-based change detection classification. The HMRF approach fully utilizes and enhances our previous change detection classification approach described in [17] by improving its robustness and sensitivity to false alarms. The method in [17] employed the Finite Gaussian Mixture (FGM) model for image classification. For example, if a ratio image X_{Ri} contains N dimensional vector of pixels with $I = \{1, 2, \ldots\ldots, N\}$ being the set of pixel indices, then for each pixel i in X_{Ri} a class label x_i is inferred using the conditional probability as shown in [17]. Each pixel in the FGM is independent from

their neighboring pixels, meaning they do not consider the relationship of pixels within its neighboring system. To improve the FGM, we modified the HMRF approach proposed by Zhang, et al. [24] and employed it. By assuming a Gaussian distribution, the HMRF model is given by

$$p(X_{Ri}|\, x_{Ni}; \theta) = \sum_{l \in L} f(X_{Ri}; \theta_l)\; q(l|\, x_{Ni}) \tag{1}$$

where $q(l|\, x_{Ni})$ is a conditional probability mass function (pmf) for a class label given that x_{Ni} are N neighbors for a pixel x_i. The segmentation process of HMRF requires an initial estimate for the class labels x_0 and initial parameters $(\theta_0 = mean(\mu_0),\ variance\left(\sigma_0^2\right))$. In this research, we used K-means clustering approach to provide these initial labels and initial parameters. The update for parameter θ_0 was estimated iteratively using our Expectation-maximization (EM) algorithm [17]. The initial labels were updated iteratively using the maximum a posteriori (MAP) algorithm. The updated label is now used to solve for $\hat{x}$ that minimizes the total posterior energy

$$\hat{x} = \underset{x \in \chi}{argmin}\{U(X_{Ri}|x) + U(x)\} \tag{2}$$

where χ is the set of all possible configurations of labels, $\hat{x}$ is the estimated class label, $U(X_{LR}|x)$ is the likelihood energy, and $U(x)$ is the prior energy function which is defined by clique potentials. A clique is a subset of nodes in which every node is connected to every other node. The clique potential was defined on pairs of neighboring pixels. We assumed that one pixel has at most eight neighboring pixels. The MAP algorithm iteration stops when Equation (2) converges or when the maximum iteration we set is reached. In this study, we classified each ratio image in X_{Ris} into three classes namely no change, moderate change, and severe change. Finally, the classified ratio image was filtered using a majority filter with mathematical morphology to remove small isolated misclassified pixels. Majority filter with mathematical morphology works by first replacing the pixels in a neighborhood using majority of their adjacent neighboring pixels and then applying opening by reconstruction followed with closing by reconstruction. The order of first doing opening by reconstruction followed by closing by reconstruction was designed to reduce noise while preserving the geometric details in the image. In this study, we set the kernel size of our majority filter to 3 and the size of our morphological kernel to 5. In the final classification map, we removed the no change class, and we multiplied each changed class (moderate change and severe change) by each crop (corn and soybean) mask derived from the CDL to estimate lodged crops per unit area.

4. Results

4.1. Sentinel-1A Backscatter Analysis for Lodging Detection

The first instances of lodging were observed in the fields on 11 August 2020 due to the windstorm on 10 August 2020. Because of the temporal frequency of Sentinel-1, lodging assessment was done on acquisitions after the lodging event. As seen in the ratio images (Figures 5 and 6), the VH polarization's backscatter (σVH) increased between the pre-lodging image and the post-lodging image. We predict the increase in value of σVH is based on two conditions:

(1) The first condition is due to volume scattering from the crops. In a healthy crop, the orientation of the crop canopy is erect. When crop lodging occurs, the orientation of the canopy elements changes, the ears and the stems bend downwards and incline against each other. Since σVH is sensitive to structural changes, when lodging occurs, the volume scattering increases.

(2) The second condition is due to the high sensitivity between the interaction of vegetation and soil (double bounce effect). When a field is lodged, the vegetation-soil double scattering increases and the σVH increases as well.

The approach for the mapping of lodging as detailed in Section 3 captures the increase in backscatter as a result of the lodging event. When the lodging is severe, condition 1 and condition

2 hold and changes in σVH are very high but when lodging is moderate, condition 1 holds and changes in σVH are moderate. The reader should note that both severe and moderate lodging are very detrimental and they will lead to yield loss. In this study, ratio images in X_{Ris} were classified into three classes. The first class, which depicts no change, comprises mostly of urban areas, healthy crops, and standing water. The second class, which depicts moderate change, contains moderately lodged fields while the third class, which depicts severe change, contains severely lodged fields (Figures 7 and 8). After classification of the lodging areas, we then quantified the amount of corn and soybean that were moderately and severely lodged (Table 2) using the CDL map.

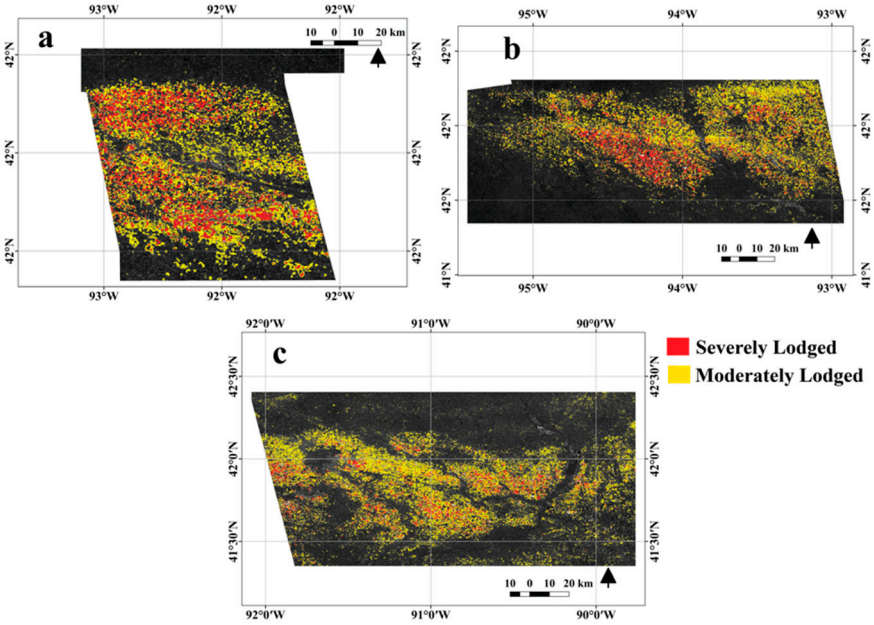

Figure 7. Lodging maps generated between (**a**) 29 July 2020 and 22 August 2020; (**b**) 3 August 2020 and 15 August 2020; (**c**) 4 August 2020 and 16 August 2020.

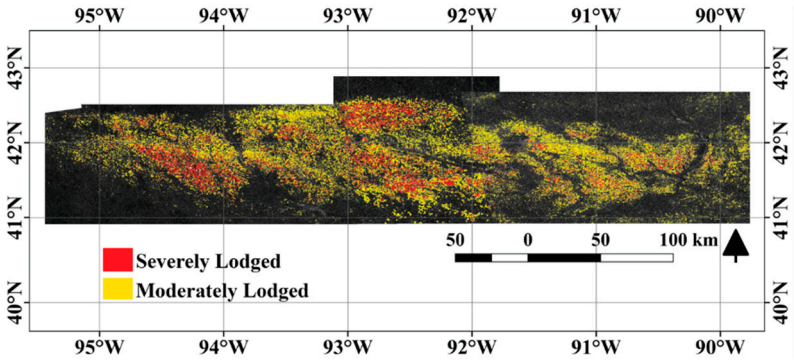

Figure 8. Spatial mosaic of all lodging maps in Figure 7a–c.

Table 2. Amount of lodged corn and soybean per unit area.

	Corn		Soybean		
	Severe (Acres)	**Moderate (Acres)**	**Severe (Acres)**	**Moderate (Acres)**	**Total (Acres)**
Figure 7a	287,238	398,821	79,246	307,482	1,072,787
Figure 7b	466,129	637,524	121,415	318,600	1,543,668
Figure 7c	326,819	442,113	120,602	318,308	1,207,842
Total (Figure 8)	1,080,186	1,478,458	321,263	944,390	
	2,558,644		1,265,653		3,824,297

4.2. Qualitative Relationship between High Wind Speed and Lodged Fields

To qualitatively check if there is a relationship between high wind speed and lodged fields, we overlaid Figures 5b and 7b with the wind speed map (Figure 2). These overlay is shown in Figure 9a,b respectively. The result showed that our estimated lodged fields followed areas with increased wind speed (Figure 9a,b). In particular, areas with wind speed of 80+ mph captured most of our estimated severely and moderately lodged fields while areas with wind speed of 60+ mph captured few lodged fields.

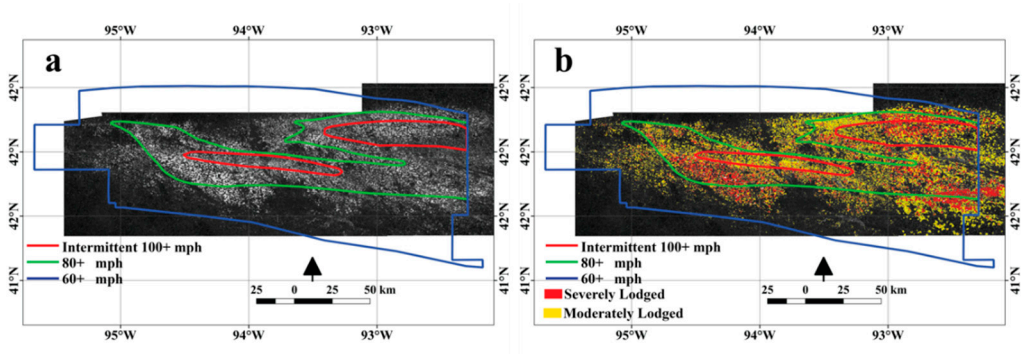

Figure 9. Example of (**a**) ratio map (Figure 5b) and (**b**) severity map (Figure 7b) overlaid with wind speed map in Figure 2.

4.3. Reliability of the Approach Employed in Mapping Lodging

To qualitatively access the performance of the Derecho lodged area mapped, we acquired eight ground truth data from field observation along the interstate I-80W. Due to limited amount of ground truth data collected, we were unable to perform extensive quantitative analysis of our method. While overlaying the eight ground truth points acquired with our lodged map, we observed that each point overlaid perfectly on an area that was lodged (Figure 10).

Furthermore, we compared an example of the lodged change detection map generated from Sentinel-1A ratio image and optical Landsat-8 ratio image by using our classification approach. The Landsat-8 ratio image was generated from the green band of pre-lodging event image acquired on 10 July 2020, and the post-lodging event image acquired on 11 August 2020 (Figure 11).

We chose the green band over every other band of Landsat-8 because the green band has a larger dynamic range which allowed for better separation of lodged and un-lodged areas. As can be seen from Figure 12, the lodging map generated from Landsat-8 ratio image and the Sentinel-1A ratio image were able to clearly detect lodging. While our approach was able to classify the Sentinel-1A ratio image into severely lodged and moderately lodged fields, we were unable to do so in the Landsat-8 ratio image. This observation showed that Sentinel-1A radar sensor has the advantage in reflecting the structural changes of lodging fields, while the Landsat-8 optical sensor only has the advantage in detecting the biochemical changes of lodging fields. All in all, for this study, we believe that the obvious feature for lodging is the structural change and the distribution pattern of lodged fields (severe

and moderate) from Sentinel-1A image were similar to the distribution pattern of the lodged fields in the Landsat-8 image.

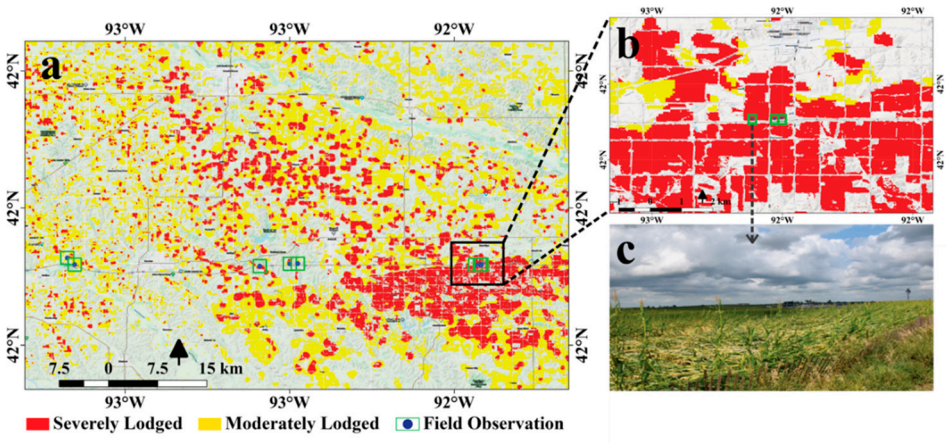

Figure 10. Location of field observations for (**a**) all the eight points and (**b**) a zoomed location for three points. (**c**) Photo for one of the field observations in "b".

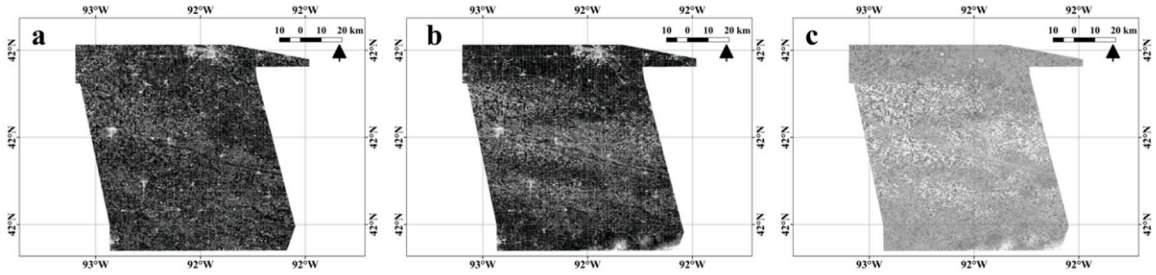

Figure 11. (**a**) Landsat-8 pre-lodging event image acquired on 10 July 2020. (**b**)Landsat-8 post-lodging event image acquired on 11 August 2020. (**c**) Ratio image generated between 10 July 2020 and 11 August 2020.

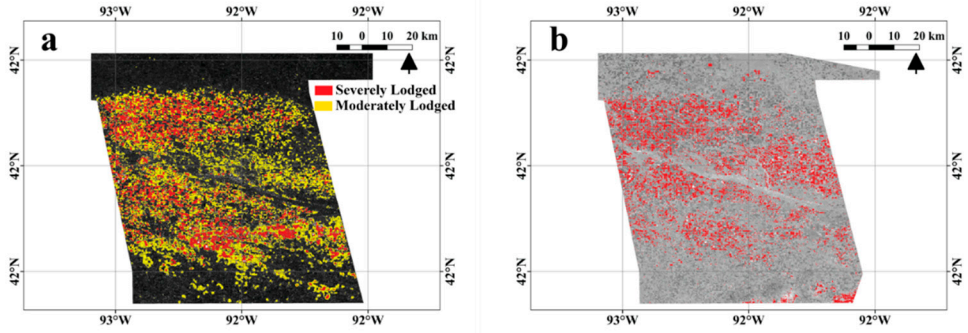

Figure 12. Severity map generated from (**a**) Sentinel-1A and (**b**) Landsat-8.

5. Discussion

5.1. Spatial-Extent of Lodging and Lodging Rate

Based on the reports by USDA Risk Management Agency (RMA), 57 counties in Iowa and Illinois were in the path of the storm which led to the Derecho lodging disaster. In the report by RMA, there are roughly 14 million acres of insured crops within those 57 counties. Also, based on the Storm Prediction Center preliminary storm reports and assessment from MODIS satellite imagery, the Iowa Department of Agriculture and Land Stewardship estimated that about 3.57 million acres of corn and 2.5 million

acres of soybeans were likely to have been impacted by the severe wind on 10 August 2020. Based on our findings using Sentinel-1A data across 52 counties, we estimated that a total of approximately 2.56 million acres of corn and approximately 1.27 million acres of soybean were impacted during the Derecho lodging disaster (Figure 8 and Table 2). Furthermore, we observed that out of the 52 counties, only 32 counties have more than 10 thousand acres per county impacted by the storm. Within these 32 impacted counties, we leveraged our proprietary yield prediction capability to quantify the yield potential prior to the storm, and we were able to quantify the total bushels lost following the windstorm. We observed the following in our findings:

(a) Corn acres impacted: ~2.36 million acres impacted out of ~4.90 million acres planted (48% acre impact).
(b) Corn bushels impacted: ~442.37 million bushels impacted out of ~918.36 million bushels expected prior to the storm (48% reduction).
(c) Soybean acres impacted: ~1.27 million acres impacted out of ~4.69 million acres planted (28% acre impact).
(d) Soybean bushels impacted: ~80.90 million bushels impacted out of ~279.00 million bushels expected prior to the storm (29% yield reduction)

As shown above and in Table 2, fields with moderate lodging were more frequent than fields with severe lodging and corn fields lodged more than soybean fields. We believe the reason for this difference is due to relatively more resistance of soybean to wind than corn.

5.2. Temporal Behavior of Un-Lodged (Healthy) and Lodged Fields throughout the Observation Period

The main difference in a field before and after lodging is the reduction of plant height. Therefore, the backscattering coefficients for lodged and un-lodged field will be different because for a lodged field, either one of the two conditions stated in Section 4.1 will hold. In this study, we compared nine randomly selected un-lodged fields to nine randomly selected lodged fields (Figure 13) using both the VH mean polarization backscatter and VV mean polarization backscatter. While observing Figure 13, on the one hand, un-lodged fields showed no change at all in both the VH and VV mean polarization backscatter. On the other hand, we saw an increase of approximately 6 dB in the VH mean polarization backscatter and 5 dB in the VV mean polarization backscatter for all the fields between the pre-lodging event date and the post-lodging event date respectively. Even though there is a slightly higher difference in the VH mean polarization backscatter, the sensitivity of VH polarization to lodging is similar to the sensitivity of VV polarization to lodging. In this study, the increase in both the VH and VV mean polarization backscatters follows the reported observations in [8]. In Chauhan, et al. [8], the authors observed a clear linear trend of increasing VH polarization backscatter and VV polarization backscatter with the increase in the lodging severity. It is worth mentioning that corn and soybean in all the fields are in the grain-filling period or plateau stage. At this stage, the height and greenness of the crop should be fairly constant, and this is why we see no change in the un-lodged fields. To further show how lodged fields and un-lodged fields differ on a large scale, we generated the VH and VV mean polarization backscatter over Dallas county in Iowa (Figure 14). By qualitatively observing the mean backscatter between the pre-lodging event date and the post-lodging event date in Figure 14, we saw an increase of approximately 3 dB in the VH mean polarization backscatter and 1 dB in the VV mean polarization backscatter. Based on the difference observed between the lodged fields and un-lodged fields in Dallas county, it is quite evident that our approach is sensitive enough to detect lodging.

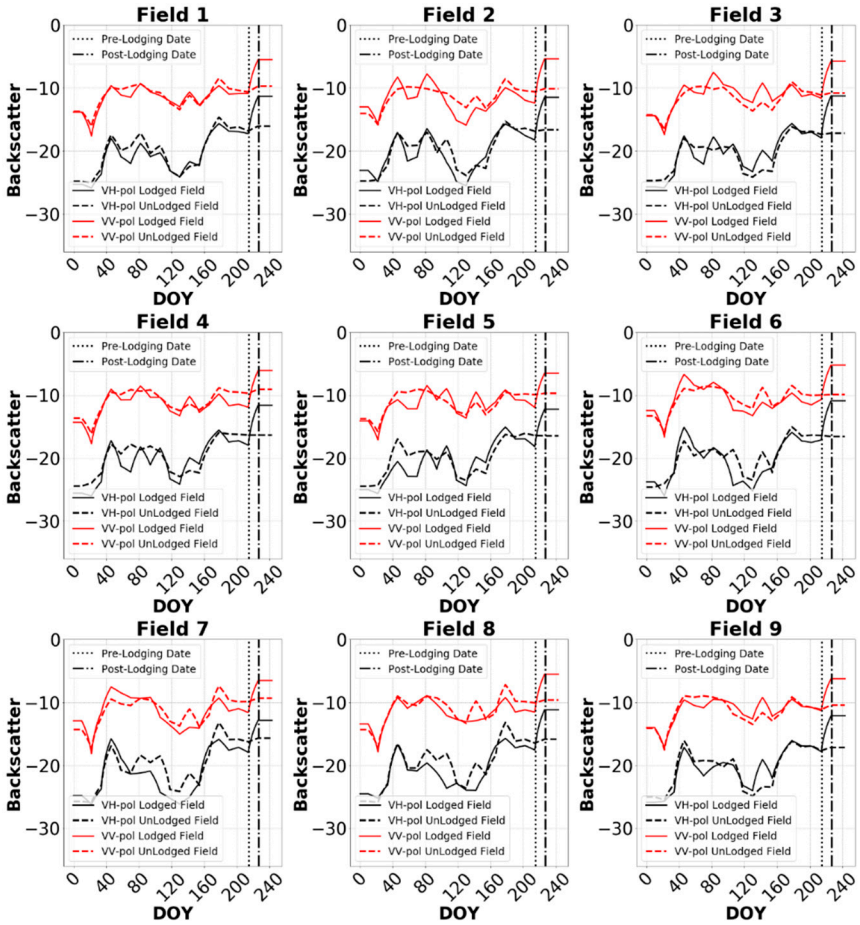

Figure 13. Time series of lodged and un-lodged fields.

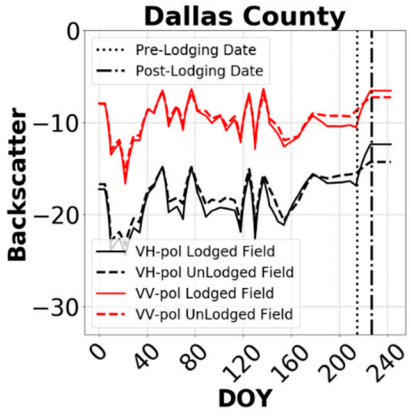

Figure 14. Time series of lodged and un-lodged fields in Dallas county, Iowa.

6. Conclusions

The potential and feasibility of using SAR data for monitoring the Derecho lodging disaster was demonstrated in this study. Though crop lodging assessment using SAR data have been shown in a few studies earlier, studies that have assessed crop lodging using satellite-based data at large spatial scale are still sparse and knowledge relating to the changes in SAR signatures was lacking in literature. With the advent of dense SAR time series from Sentinel-1 and proposed missions like NASA ISRO Synthetic Aperture Radar (NISAR), there is an increased interest in exploring SAR for lodging identification. The main conclusions of this study are summarized below.

(1) The modified change detection approach used was shown to be capable of providing near real-time monitoring of the Derecho lodging disaster by generating detailed parameters, such as backscatter changes, lodging extent, and lodging rate in corn and soybean. The generated lodging extent maps from SAR showed both severely and moderately damaged fields. The use of CDL also allowed the estimation of lodged crop per unit area, showing relatively more lodging in corn fields than soybean fields. We believe the sensitivity of corn to lodging was caused by its unique structural characteristics (long vertical orientation of its stalk). We estimated that a total of approximately 2.56 million acres of corn and approximately 1.27 million acres of soybean were impacted during the Derecho lodging disaster.

(2) The modified change detection approach used was reliable and the reliability can be seen by the similar distribution patterns of lodged fields in the Sentinel-1A imagery and Landsat-8 imagery. Furthermore, the generated lodged field maps show correlation with areas of extreme wind speed.

(3) The backscatter difference between the timeseries of lodged and un-lodged (healthy) fields differ. Our analyses from nine fields showed almost no change between the pre-lodging event image and post-lodging event image of an un-lodged field while we noted an approximately 6 dB increase in the VH mean polarization backscatter and 5 dB increase in the VV mean polarization backscatter for all the fields between the pre-lodging event date and the post-lodging event date. When we aggregated all the un-lodged fields and the lodged fields across Dallas county, we saw an increase of approximately 3 dB in the VH mean polarization backscatter and 1 dB in the VV mean polarization backscatter between the pre-lodging event date and the post-lodging event date. Taken together, these results suggest that differences in VH polarization and VV polarization can serve as useful lodging indicators at parcel- and landscape-level and enable rapid mapping of widespread lodging events using SAR data.

Taken together, the results and the insights from this study demonstrate the practicability of using high resolution SAR remote sensing data for large scale identification of crop lodging. The approach employed is simple, effective, and can help decision-makers obtain critical information on lodging identification to support precision management in order to provide effective emergency relief. Future studies will evaluate if there is any improvement in the lodging detection performance when SAR and multispectral datasets are fused. We will also undertake quantitative measures to further validate our results. Using the validated crop lodging area in this study as a reference, we will investigate the use of deep learning models to generate a standard near-real time framework for crop lodging assessment. We will also explore the use of Gamma distribution for fitting the EM algorithm in the HMRF rather than Gaussian distribution. With adequate ground truth information and further validation, large-scale crop lodging assessment can improve crop yield forecasting and crop insurance, ultimately benefitting food production and food security initiatives.

Author Contributions: Conceptualization, O.A.A.; methodology, O.A.A.; software, O.A.A.; validation, O.A.A. and H.L.; formal analysis, O.A.A.; investigation, O.A.A. and H.L.; data curation, O.A.A. and A.D.S.; writing—original draft preparation, O.A.A.; writing—review and editing, O.A.A., H.L., J.J., R.P., A.S., and S.P.K.; visualization, O.A.A.; supervision, A.S.; project administration, R.P. and A.S.; funding acquisition, A.S. All authors have read and agreed to the published version of the manuscript.

Funding: This work was supported by Corteva Agriscience™.

Conflicts of Interest: The authors declare no conflict of interest.

References

1. Pinthus, M.J. Lodging in wheat, barley, and oats: The phenomenon, its causes, and preventive measures. In *Advances in Agronomy*; Elsevier: Amsterdam, The Netherlands, 1974; Volume 25, pp. 209–263.
2. Wu, W.; Ma, B.L. A new method for assessing plant lodging and the impact of management options on lodging in canola crop production. *Sci. Rep.* **2016**, *6*, 31890. [CrossRef] [PubMed]
3. Xue, J.; Gou, L.; Zhao, Y.; Yao, M.; Yao, H.; Tian, J.; Zhang, W. Effects of light intensity within the canopy on maize lodging. *Field Crop. Res.* **2016**, *188*, 133–141. [CrossRef]

4. Nielsen, B.; Colville, D. Stalk Lodging in corn: Guidelines for Preventive Management. Available online: https://www.extension.purdue.edu/extmedia/ay/ay-262.html (accessed on 30 October 2020).
5. Kong, E.; Liu, D.; Guo, X.; Yang, W.; Sun, J.; Li, X.; Zhan, K.; Cui, D.; Lin, J.; Zhang, A. Anatomical and chemical characteristics associated with lodging resistance in wheat. *Crop J.* **2013**, *1*, 43–49. [CrossRef]
6. Chauhan, S.; Darvishzadeh, R.; Boschetti, M.; Pepe, M.; Nelson, A. Remote sensing-based crop lodging assessment: Current status and perspectives. *Isprs J. Photogramm. Remote Sens.* **2019**, *151*, 124–140. [CrossRef]
7. Shah, S.; Chang, X.; Martin, P. Effect of dose and timing of application of different plant growth regulators on lodging and grain yield of a scottish landrace of barley (bere) in orkney, scotland. *Int. J. Environ. Agric. Biotechnol.* **2017**, *2*, 238871. [CrossRef]
8. Chauhan, S.; Darvishzadeh, R.; Lu, Y.; Boschetti, M.; Nelson, A. Understanding wheat lodging using multi-temporal sentinel-1 and sentinel-2 data. *Remote Sens. Environ.* **2020**, *243*, 111804. [CrossRef]
9. Chauhan, S.; Darvishzadeh, R.; Lu, Y.; Stroppiana, D.; Boschetti, M.; Pepe, M.; Nelson, A. Wheat lodging assessment using multispectral uav data. *Int. Arch. Photogramm. Remote Sens. Spat. Inf. Sci.* **2019**, 235–240. [CrossRef]
10. Han, D.; Yang, H.; Yang, G.; Qiu, C. 2017 SAR in Big Data Era: Models, Methods and Applications (BIGSARDATA). In *Monitoring Model of Corn Lodging Based on Sentinel-1 Radar Image*; IEEE: New York, NY, USA, 2017; pp. 1–5.
11. Zhao, L.; Yang, J.; Li, P.; Shi, L.; Zhang, L. Characterizing lodging damage in wheat and canola using radarsat-2 polarimetric sar data. *Remote Sens. Lett.* **2017**, *8*, 667–675. [CrossRef]
12. Meyer, F.; McAlpin, D.; Gong, W.; Ajadi, O.; Arko, S.; Webley, P.; Dehn, J. Integrating sar and derived products into operational volcano monitoring and decision support systems. *Isprs J. Photogramm. Remote Sens.* **2015**, *100*, 106–117. [CrossRef]
13. Shu, M.; Zhou, L.; Gu, X.; Ma, Y.; Sun, Q.; Yang, G.; Zhou, C. Monitoring of maize lodging using multi-temporal sentinel-1 sar data. *Adv. Space Res.* **2020**, *65*, 470–480. [CrossRef]
14. Chauhan, S.; Darvishzadeh, R.; Boschetti, M.; Nelson, A. Estimation of crop angle of inclination for lodged wheat using multi-sensor sar data. *Remote Sens. Environ.* **2020**, *236*, 111488. [CrossRef]
15. Yang, H.; Chen, E.; Li, Z.; Zhao, C.; Yang, G.; Pignatti, S.; Casa, R.; Zhao, L. Wheat lodging monitoring using polarimetric index from radarsat-2 data. *Int. J. Appl. Earth Obs. Geoinf.* **2015**, *34*, 157–166. [CrossRef]
16. Chen, J.; Li, H.; Han, Y. Fifth International Conference on Agro-Geoinformatics (Agro-Geoinformatics). In *Potential of Radarsat-2 Data on Identifying Sugarcane Lodging Caused by Typhoon*; IEEE: New York, NY, USA, 2016; pp. 1–6.
17. Ajadi, O.A.; Meyer, F.J.; Webley, P.W. Change detection in synthetic aperture radar images using a multiscale-driven approach. *Remote Sens.* **2016**, *8*, 482. [CrossRef]
18. Baier, G.; Rossi, C.; Lachaise, M.; Zhu, X.X.; Bamler, R. A nonlocal insar filter for high-resolution dem generation from tandem-x interferograms. *IEEE Trans. Geosci. Remote Sens.* **2018**, *56*, 6469–6483. [CrossRef]
19. Deledalle, C.-A.; Denis, L.; Tupin, F.; Reigber, A.; Jäger, M. Nl-sar: A unified nonlocal framework for resolution-preserving (pol)(in) sar denoising. *IEEE Trans. Geosci. Remote Sens.* **2014**, *53*, 2021–2038. [CrossRef]
20. Kasetkasem, T.; Varshney, P.K. An image change detection algorithm based on markov random field models. *IEEE Trans. Geosci. Remote Sens.* **2002**, *40*, 1815–1823. [CrossRef]
21. Zhao, Q.-H.; Li, X.-L.; Li, Y.; Zhao, X.-M. A fuzzy clustering image segmentation algorithm based on hidden markov random field models and voronoi tessellation. *Pattern Recognit. Lett.* **2017**, *85*, 49–55. [CrossRef]
22. Yang, M.; Yi, C. A novel method of ship detection in high-resolution sar images based on gan and hmrf models. *Prog. Electromagn. Res.* **2019**, *83*, 77–82. [CrossRef]
23. Boryan, C.; Yang, Z.; Mueller, R.; Craig, M. Monitoring us agriculture: The us department of agriculture, national agricultural statistics service, cropland data layer program. *Geocarto Int.* **2011**, *26*, 341–358. [CrossRef]
24. Zhang, Y.; Brady, M.; Smith, S. Segmentation of brain mr images through a hidden markov random field model and the expectation-maximization algorithm. *IEEE Trans. Med Imaging* **2001**, *20*, 45–57. [CrossRef] [PubMed]